Surface structure of Kevlar® fiber studied by atomic force microscopy and inverse gas chromatography

S. Rebouillat[a,*], J.C.M. Peng[b], J.-B. Donnet[b]

[a]DuPont de Nemours International S.A., European Technical Centre, 146, route du Nant d'Avril-Meyrin, CH-1218 Le Grand-Saconnex, Geneva, Switzerland
[b]Ecole Nationale Supérieure du Chimie—Université de Haute-Alsace, 3, rue A. Werner, 68093 Mulhouse Cedex, France
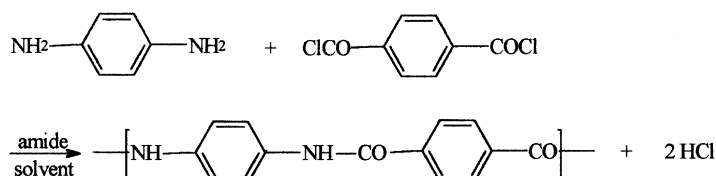
Abstract

Kevlar® fiber surface structure was primarily and directly observed in the filament configuration by the tapping mode atomic force microscopy (AFM). The microfibrils feature was observed with an average width of 500 nm, composed of various types of periodical units of an average size 50 nm in a pleating appearance. At the less crystalline spot on the Kevlar® fiber surface, the periodical organizations exhibit the skin-core-like differentiation. In contrast, at the highly crystalline spot, the periodicity is more uniformly arranged by a rectangular network manner. Inverse gas chromatography (IGC) was used as a tool to investigate the surface structure heterogeneity by calculating the surface energy of different types of probes adsorbed on the Kevlar® fiber surface. The energy sites distribution plot of n-hexylamine adsorption at finite dilution exhibits a two-adsorbing-peaks curve. At the higher energy site, a possible hydrogen-bonding interaction was proposed between n-hexylamine and oxygen-containing groups formed at the less crystalline surface. According to the AFM and IGC results, a Kevlar® fiber surface organizations model at the nanometer scale was proposed. © 1999 Elsevier Science Ltd. All rights reserved.

Keywords: Kevlar® fiber; Atomic force microscopy; Tapping mode

1. Introduction

Kevlar® (a DuPont registered trade mark) fiber exhibits an excellent thermal stability, as well as superior tensile strength and modulus. The chemical composition of Kevlar® fiber is based on poly(p-phenylene terephthalamide) (PPTA) which is synthesized by terephthaloyl-chloride and p-phenylene diamine in a solvent at a low temperature polycondensation [1,2].

Kevlar® fiber has a highly ordered molecular structure with high crystalinity. Observed from XRD data, the angle is 160° between the amide and carbonyl end groups and the characteristic distance of adjacent polymer chains is 3 Å [2]. Thus, a strong hydrogen-bonding which links the adjacent chains into the lattice planes is evidenced. The fiber is also characterized by a pleated arrangement along the fiber axis, the angle between pleats reported [3] being around 170°. The unit of these pleated appearance is between 500 and

600 nm, observed by several groups [4–6] using the electron microscope dark-field image and X-ray diffraction techniques. Dobb et al. [4] reported a PPTA structure with a pleat unit 250 nm along the fiber axis and arranged

* Corresponding author. Tel.: + 41-22-717-5889; fax: + 41-22-717-6868.
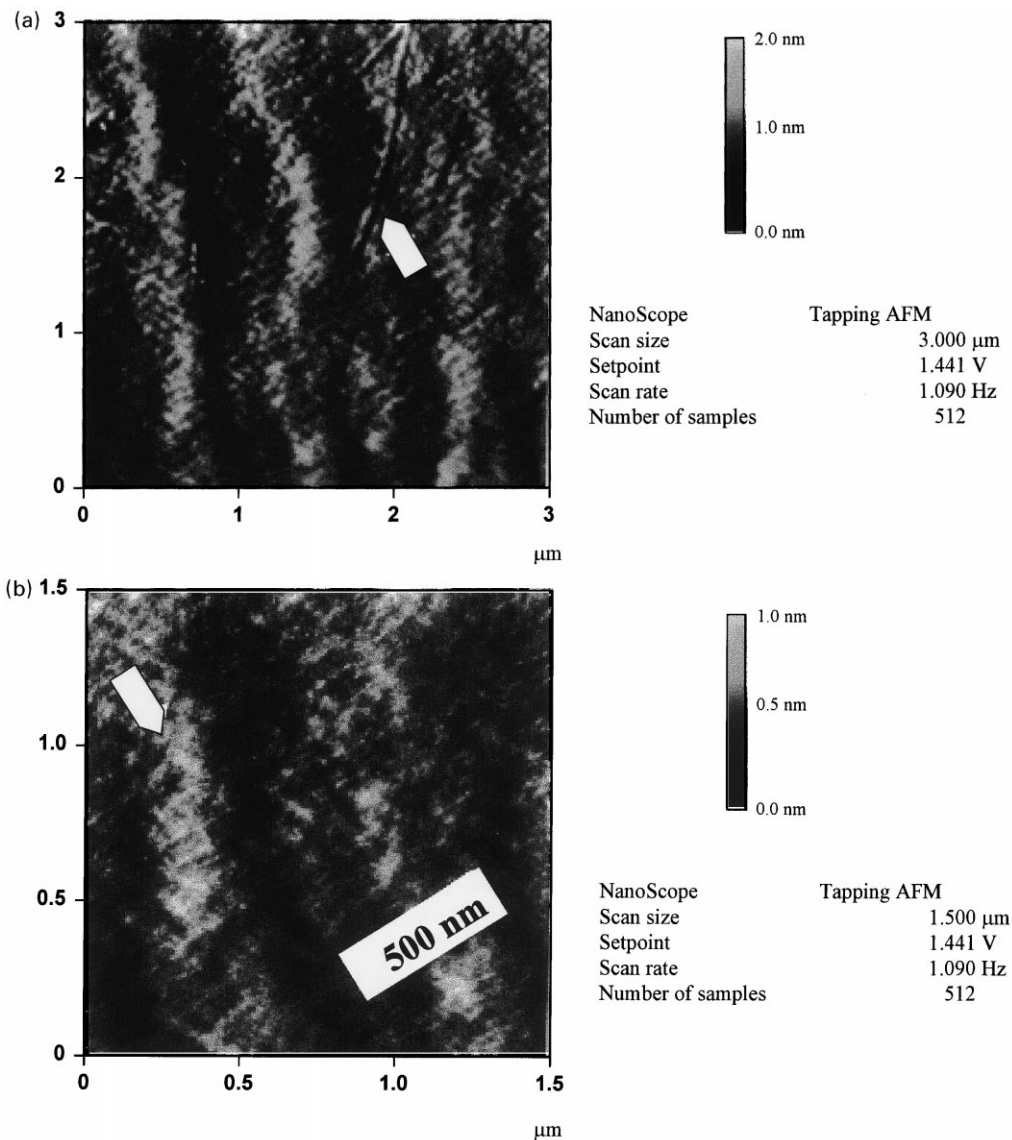 E-mail address: serge.rebouillat@che.dupont.com (S. Rebouillat)

Fig. 1. Surface morphology of Kevlar® K673 fiber at the micrometer scale, (a) 3 μm × 3 μm, topview; (b) 1.5 μm × 1.5 μm, topview, the arrow indicates microfibril direction.

regularly in the radial direction. Li et al. [6] described a supermolecular structure with a pleat average length 220 nm along the axial direction and found a hydrogen-bonded structure in the radial direction. The overall fiber structure is fibrillar. Panar et al. [7] indicated that the fibrils are oriented along the fiber axis with a width of about 600 nm and up to several centimeters long.

The invention of atomic force microscopy (AFM) makes it as a new and attractive research tool, and recently this technique has been applied to study the Kevlar® fiber surface microstructure [8–10], as well as the morphology of other types of organic polymer fibers, such as ultrahigh molecular weight polyethylene fibers [11]. In AFM application, the mechanical deformation of the surface

when operated by the contact mode due to a high tip/sample forces often occurs in the soft materials, such as polymers [12]. In contrast, the tapping mode AFM has recently been developed [12], and the topography of samples can be measured by a small piezoelectric element where the tip is driven into an oscillation at its resonant frequency. In this mode, short, intermittent contacts between the sample surface and the tip eliminates the shear forces which can damage soft samples and reduce image resolution. In the present study, tapping mode AFM was employed as an ongoing effort [10] to study the microstructure of PPTA fibers of a direct observation at the fiber filament configuration, with no risk of interference of any mixing component if the AFM sample is microtomed when the
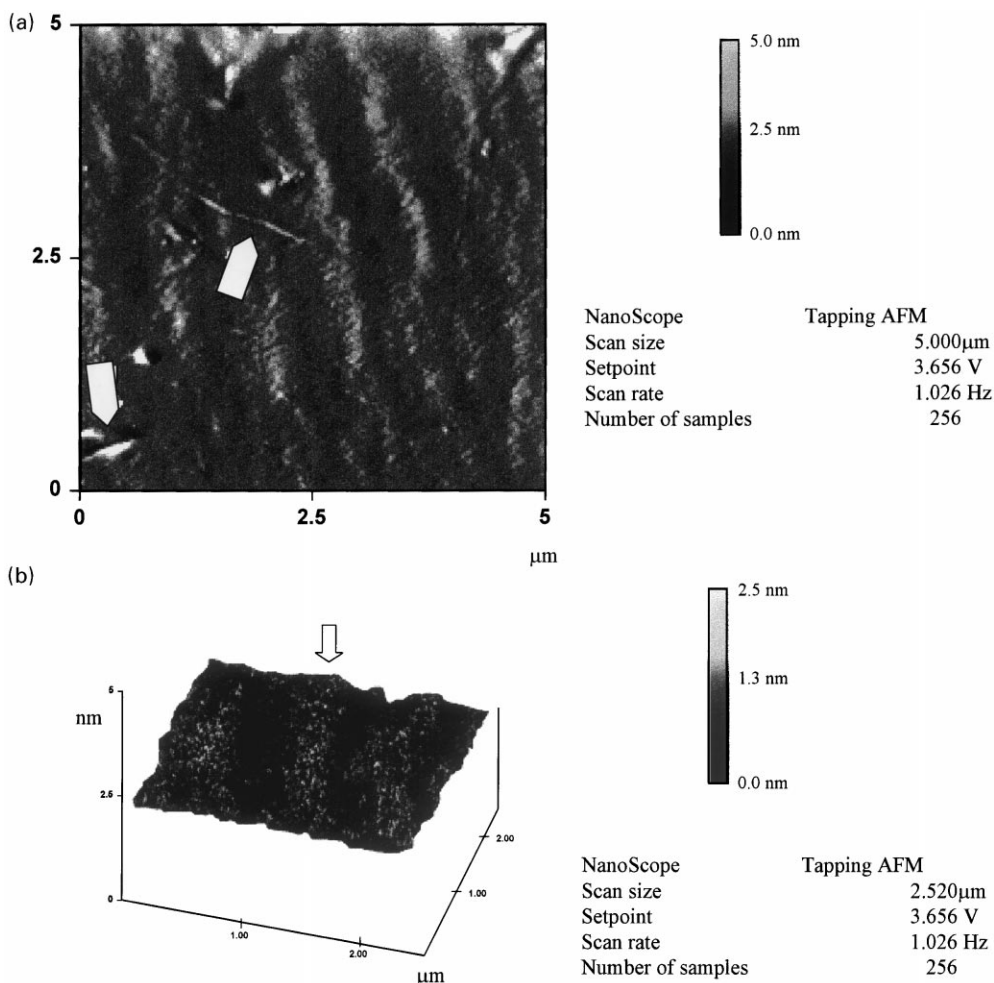
Fig. 2. Surface morphology of Kevlar® K671 fiber at the micrometer scale, (a) 5 μm × 5 μm, topview, the arrows indicate impurities or defects; (b) 2.5 μm × 2.5 μm, line plot, the arrow indicates microfibril direction.

fiber is embedded in the epoxy [8,9]. The authors tried to confirm or clarify different theories of various structure models described in the literature [4,6,13].

Inverse gas chromatography (IGC) was previously applied to study the surface energy distribution and specific interaction with non-polar and polar probes of Kevlar® fiber surface [14,15]. We attempt to use the IGC technique to investigate the surface energy heterogeneity and to further evaluate the correlation between the Kevlar® fiber surface energy and surface morphology. There are two approaches, infinite and finite concentration methods, used in the Kevlar® fiber surface energy characterization. The theoretical concepts of IGC at infinite and finite dilution have been thoroughly discussed in the previous publication [15]. At finite dilution method, the energy site distribution function $\chi(\varepsilon)$ was calculated according to the Robson's model [16,17]. The fiber surface energy heterogeneity can be theoretically described as a distribution function $\chi(\varepsilon)$ of the surface sites that correspond to the absorbed probe molecule energy level ε. Both expressions are defined in the following:

$$\chi(\varepsilon) = -\left(\frac{P}{RT}\right)^2 \frac{\partial V_n(P, T)}{\partial P},$$

$$\varepsilon = -RT \ln \frac{P}{K},$$

where K is pre-exponential factor of Henry's constant, and can be expressed by $K = 1.76 \times 10^4 \, (MT)^{1/2}$. M is the molecular weight of the probe, T is the experimental temperature and P the partial pressure of the adsorbate.

2. Instrumentation and samples

A commercial scanning force microscope (NanoScope III, Digital Instruments, Inc.) was used, and the tip was made of Si. The silicon probe is considerably stiffer than the contact mode probe, silicon nitride. The Si probe
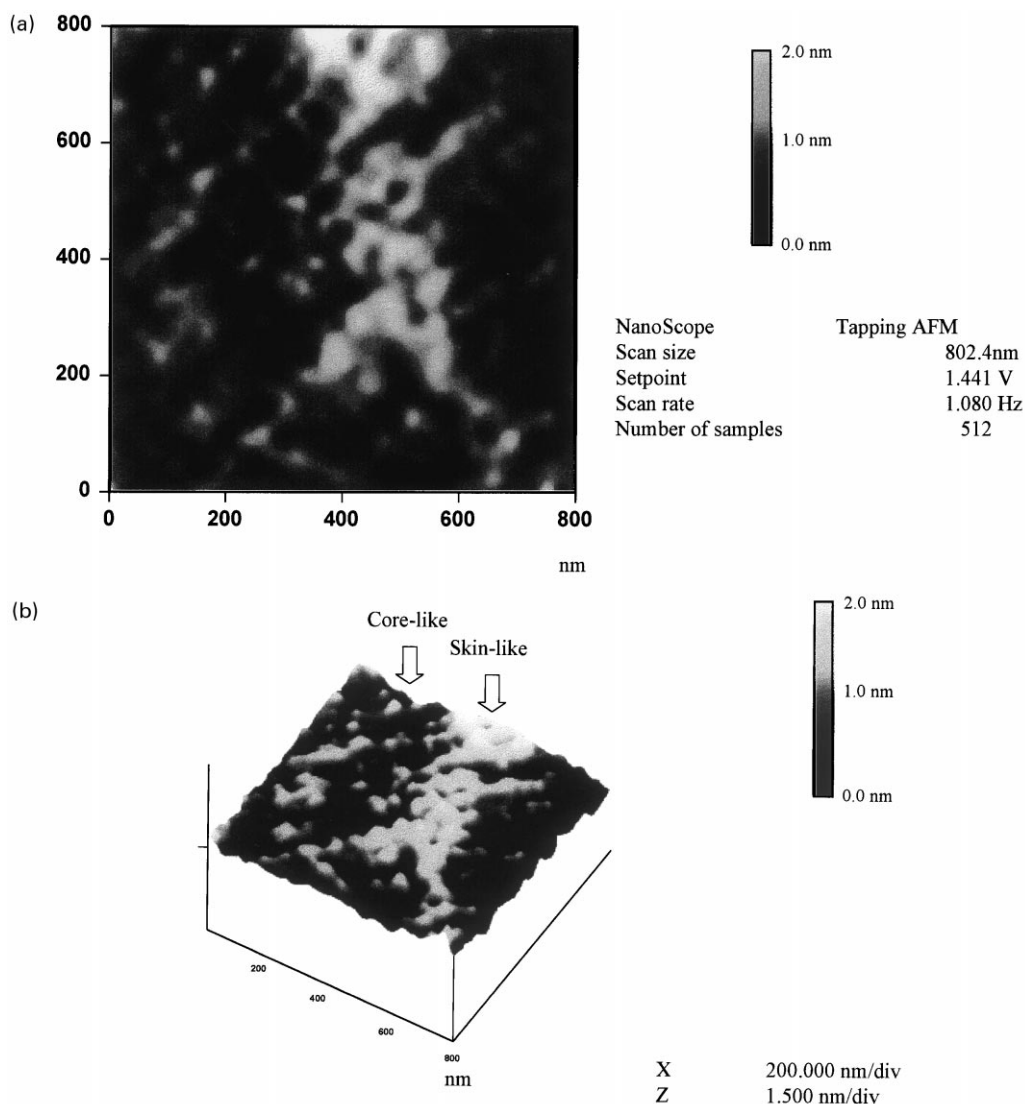
Fig. 3. Surface morphology of Kevlar® K673 fiber at the nanometer scale, (a) 800 nm × 800 nm, topview; (b) 800 nm × 800 nm, 3D surface plot; (c) surface depth features analysis of image in Fig. 3(a).

oscillates at a high-frequency ($\geq$ 100 KHz) and possesses sufficient energy to overcome the surface tension forces between sample surface and tip. The scanner used is AS-12 E type which permits a scan size from nanometers up to 10 μm × 10 μm. Three types of PPTA fibers, DuPont Kevlar® K671 and K673 fibers used in the AFM study, and DuPont Kevlar® K673 fiber in the IGC study, were ultra-clean samples without any post finished surface treatment. These three types of DuPont Kevlar® fibers were produced during the fiber manufacturing processes. The fiber yarn is composed of 1000 filaments of an average diameter of 12 μm. The PPTA fibers were observed in filaments configuration directly in air at room temperature, without any further embedding in epoxy resin. All the AFM micrographs shown below are raw data without any image analysis treatment.

"HI-EFF" grade stainless steel tubing with a diameter of 4.4 mm was cut into a 60 cm long segment and pre-cleaned in a 10% HNO_3 solution for 1 h before fiber packing. After rinsed with acetone and distilled water the column was heated in the oven at 120°C overnight. 5.1 g of Kevlar® fibers partially fibrillated were filled into the column, then were mounted on an Intersmat IGC 121 DFL gas chromatograph equipped with a hydrogen flame ionization detector (FID). Helium gas was used as a carrier with a flow rate of 26 ml/min, determined by the method of theoretical plate number [18]. Before IGC measurements were performed at 50°C, the fiber packed column was conditioned at 180°C under He gas for 20 h to eliminate impurities or physical adsorbed materials on the Kevlar® fiber surface. For the experiments at finite concentration, n-octane was chosen as the non-polar probe and n-hexylamine was chosen as
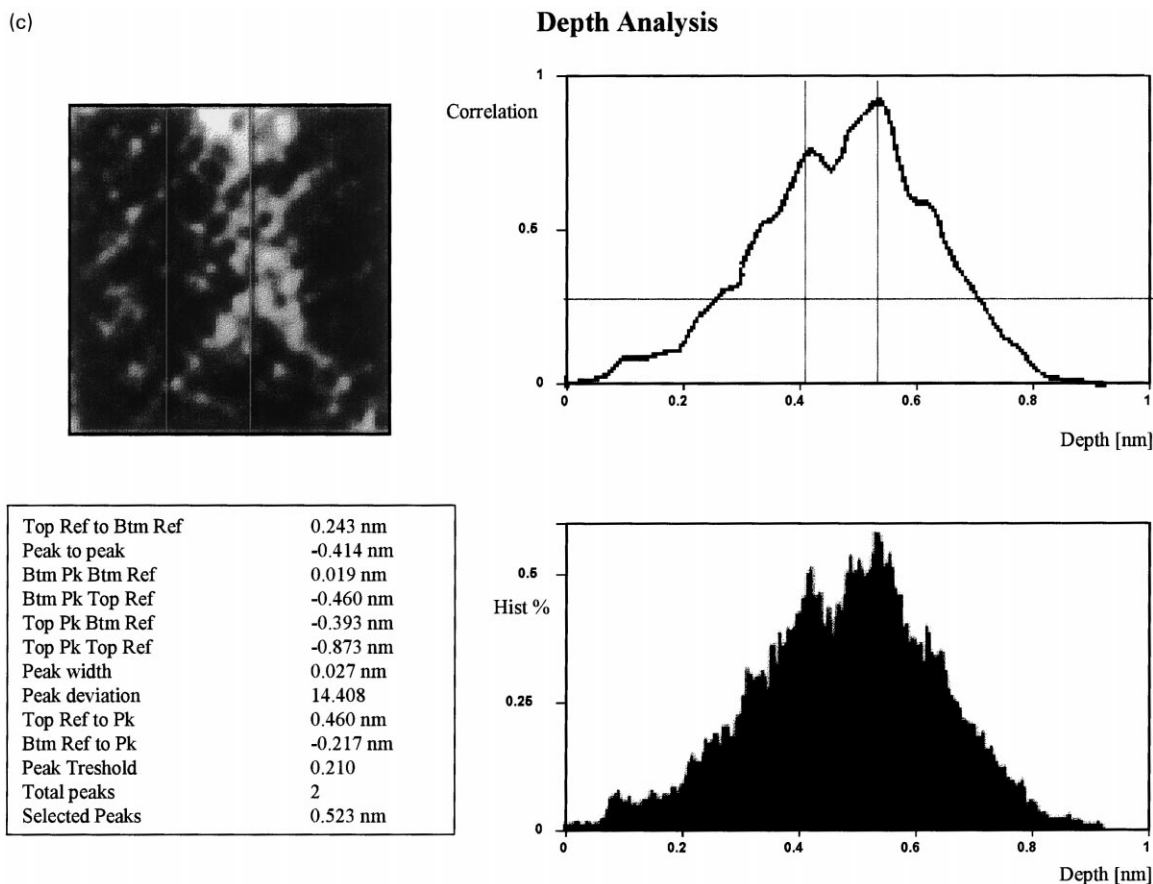
(c)

Depth Analysis

Top Ref to Btm Ref	0.243 nm
Peak to peak	-0.414 nm
Btm Pk Btm Ref	0.019 nm
Btm Pk Top Ref	-0.460 nm
Top Pk Btm Ref	-0.393 nm
Top Pk Top Ref	-0.873 nm
Peak width	0.027 nm
Peak deviation	14.408
Top Ref to Pk	0.460 nm
Btm Ref to Pk	-0.217 nm
Peak Treshold	0.210
Total peaks	2
Selected Peaks	0.523 nm

Fig. 3. (*continued*)

3. Results and discussion

Fig. 1(a) illustrates a typical longitudinal section image of a Kevlar® K673 fiber by 3 μm × 3 μm, and the microfibrils structure feature (pointed by the arrow) is clearly seen along the fiber axis. In Fig. 1(b), details of the microfibril structure, i.e. a pleating arrangement perpendicular the fiber axis, can be recognized. On the basis of surface profile analysis, the width of the microfibril is in the neighborhood of 500 nm, and this observation is consistent with the previous data [13]. Similar results were observed on the Kevlar® K671 fiber. The microfibril structure feature is also clearly seen as illustrated in Fig. 2(a) (5 μm × 5 μm size, topview) and Fig. 2(b) (2.5 μm × 2.5 μm, line plot), where the microfibrils in Fig. 2(b) is particularly represented such as the ribs (pointed by the arrow) of mountains by the line plotting. Twisted lines lying across the surface or the rod-shape boundaries mounted into the Kevlar® surface (pointed by the arrows) were clearly seen at the micrometer scale on

both the AFM micrographs of Figs. 1(a) and 2(a). These observations might be interpreted as impurities or defects on the Kevlar® fiber surface that come from during the manufacturing process. The AFM image of Figs. 1 and 2 show the good reproducibility of the technique as both the corresponding samples were obtained separately during the manufacturing of Kevlar®.

The surface microfibril features of Kevlar® fibers have previously been observed by AFM contact mode [8–10]; however, to our knowledge, the repeated pleating appearance unit was not easily seen in a distinguished configuration but more likely twisted and overlapped due to the mechanical deformation limitation of the contact mode operation. In contrast, the tapping mode technique offers a short and intermittent contact between the tip and Kevlar® surface, and thus the pleated periodical structure with minimized deformation can be verified. These units are clearly seen to be cross-linked in the radial direction, and such a 2D network may be originated from the hydrogen-bonding effect.

Fig. 3 shows the Kevlar® fiber structure in the nanometer scale, and the skin-core-like structure feature can be distinguished, as has been previously reported by AFM [9]. Pointed by the arrow, the skin-like fibrils
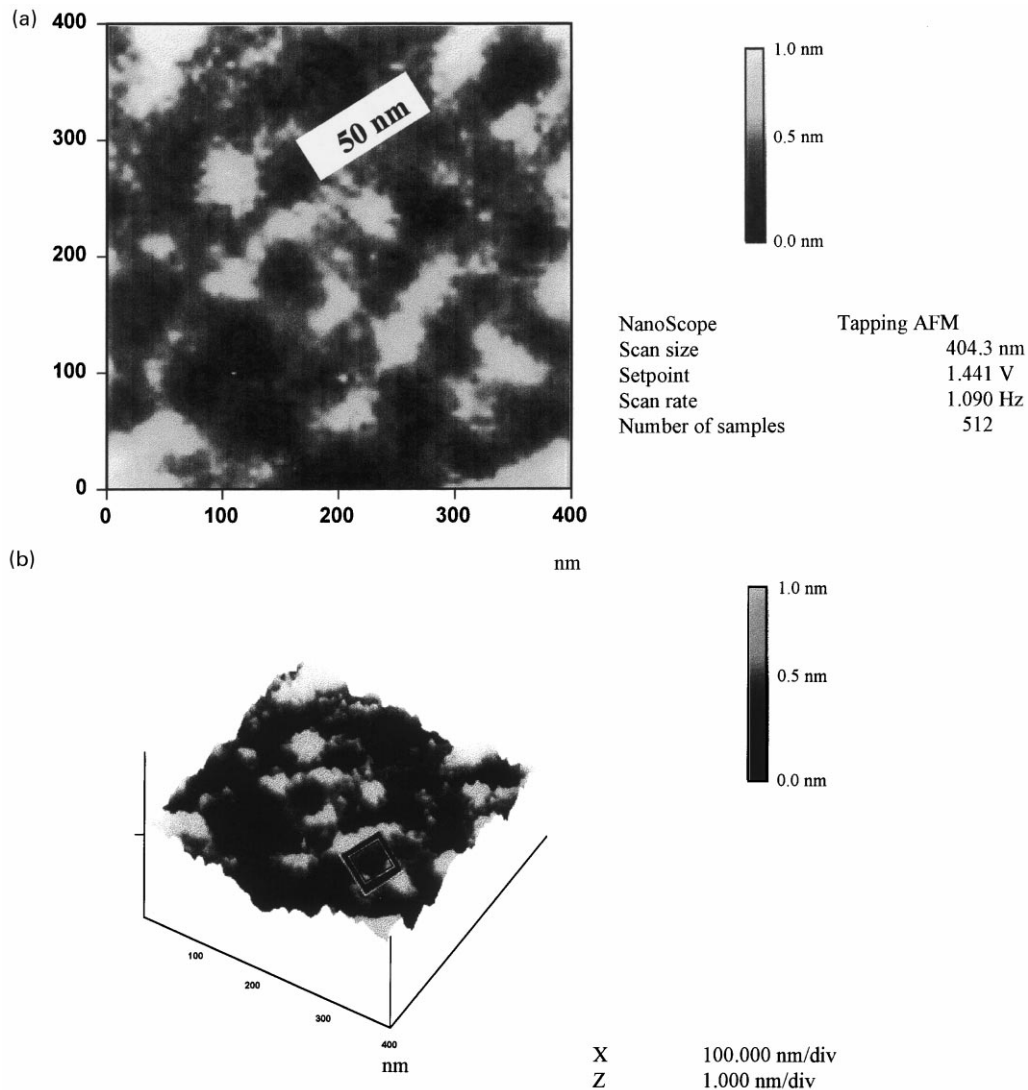
Fig. 4. Pleated periodical structure arrangements from a highly ordered crystalline zone of Kevlar® K673 fiber surface, 400 nm × 400 nm, (a) 2D topview; (b) 3D surface plot.

appear to be indistinct and merged among each other, and this observation agrees with the previous data [8]. A close-up view of the 3D image (skin-like and core-like zones were pointed by arrows) in Fig. 3(b), there are more voids or defects present in the core-like region than in the skin-like zone (the arrow points one of the void). The depth features of image in Fig. 3(a) is further analyzed as shown in Fig. 3(c). The depth analysis configuration includes a topview image, two histograms, and depth data is displayed at the bottom left corner. The bottom histogram displays the raw depth data, and the top histogram displays a lowpass, Gaussian-filtered version of the same data that removes noise from the data curve and averages the curve's profile. The depth data in the histogram is distributed proportional to its occurrence within the defined bounding box. As shown in Fig. 3(c), there is a two-peak

curve occurred in the defined bounding box. The left vertical cursor on the peak corresponding to the shallowest of the two featured to be compared, on the other hand, the right cursor corresponding to the deepest. This AFM observation and analysis might be interpreted as the typical skin-like (the shallowest peak)/core-like (deepest peak) features of PPTA fibers. Panar et al. [13] proposed a skin-core model based on the SEM evidence and indicated that the core region of PPTA fibers exhibited a disordered and imperfect packing, thus voids were easily formed there. In contrast, the skin fibers were more tightly packed and uniform. The skin-core-like structure terminology defined in our AFM observation is based on the surface differentiation at the nanometer scale, different from the description of Panar's model, but the AFM surface morphology seems to have a similar features as Panar or others

(a)

Bearing Analysis

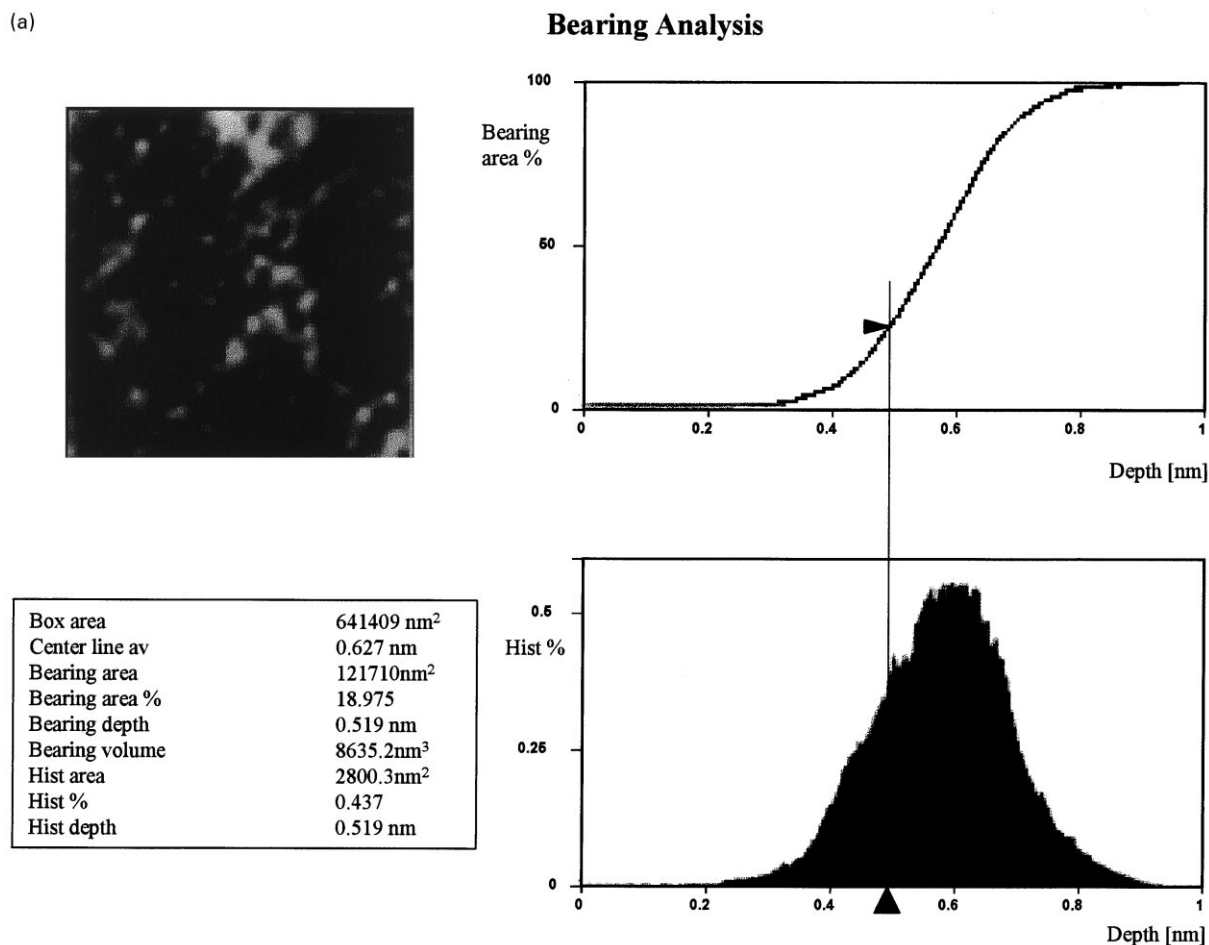|	
Box area	641409 nm^2
Center line av	0.627 nm
Bearing area	121710nm^2
Bearing area %	18.975
Bearing depth	0.519 nm
Bearing volume	8635.2nm^3
Hist area	2800.3nm^2
Hist %	0.437
Hist depth	0.519 nm

Fig. 5. Surface bearing analysis of the distribution of surface height over the AFM micrographs in (a) Fig. 3(a); (b) Fig. 5(a), (c) bearing analysis results compare of (a) and (b).

described in the literature [4,6,13]. The fibrils are composed of periodical organizations which are more tightly connected and interlocked in the skin-line zone. However, the core-like fibrils appear loose and the pleated chains are disconnected across the defect zones.

Fig. 4(a) is another image of Kevlar® fiber, clearly indicating that on some spot the periodical structures are arranged in an orderly rectangular network manner. Fig. 4(b) is the 3D surface plot of the Fig. 4(a) micrograph. As shown in Fig. 4(a), the average size of periodical unit structure is calculated to be about 50 nm, and this value confirms Vancso's et al. [8] observation. With the surface roughness comparison calculated by the program of NanoScope III between the images in Figs. 3(a) and 4(a), the surface morphology of Fig. 4(a) is more flat than the other. In contrast, another surface analysis function, called "bearing", provides a method of plotting and analyzing the distribution of surface height over a sample. This measurement provides additional information beyond standard roughness measurements. By utilizing bearing analysis, it is possible to calcu-

late what percentage of the surface lies above or below a given height. The bearing analysis results of the image in Figs. 3(a) and 4(a) are illustrated in Fig. 5(a) and (b), respectively. The bearing ratio curve is plotted as the total percentage of the surface above a reference plane as a function of the depth of that plane below the highest point in the image. Once obtaining the bearing analysis results on two images, it is possible to compare any height differences between them by using the *Bearing Compare* function to generate a composite height histogram and bearing ratio curve. To ensure an accurate comparison between images, the files were treated by the *Plane Fit* modification to have the surfaces at the same altitudes. Fig. 5(c) displays the results of the bearing compare analysis that the difference bearing ratio curve is calculated as the files of Fig. 5(a) minus Fig. 5(b). As shown, the subtracted curve is located to the right of the center line, indicating the profile in Fig. 3(a) is on average *higher* than that of Fig. 4(a). Therefore, based on the roughness and bearing compare analysis, it was suggested that this highly organized periodical arrangements observed in Fig. 4(a), might be obtained
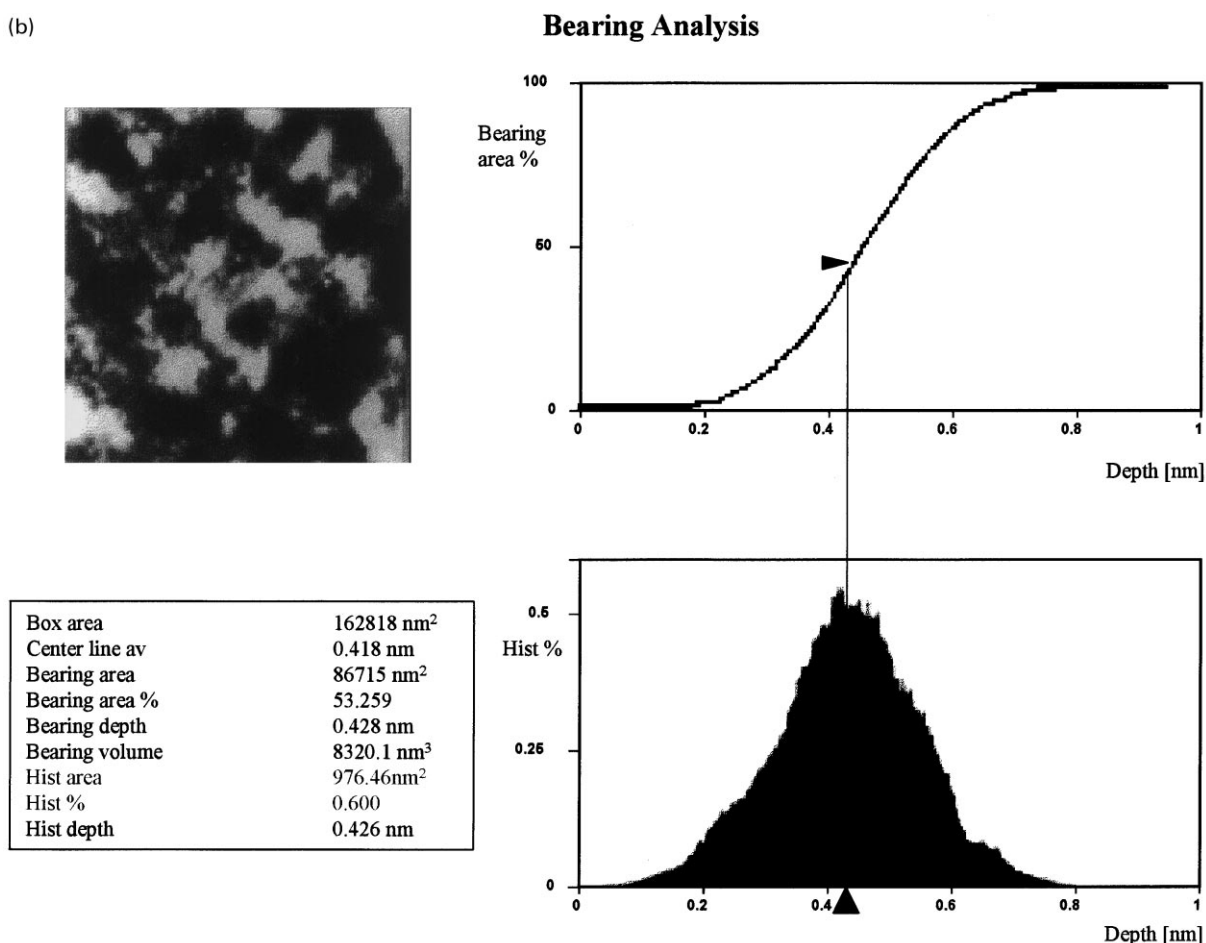
(b)

Bearing Analysis

Box area	162818 nm^2
Center line av	0.418 nm
Bearing area	86715 nm^2
Bearing area %	53.259
Bearing depth	0.428 nm
Bearing volume	8320.1 nm^3
Hist area	976.46nm^2
Hist %	0.600
Hist depth	0.426 nm

Fig. 5. (*continued*)

from a flat and less rough region, such as a highly ordered crystalline zone on the Kevlar® fiber surface.

IGC operated at finite concentration was used as a tool to study the surface energy distribution of K673 Kevlar® fiber and to further evaluate the relationship with the surface morphology. Fig. 6(a) and (b) illustrate the energy distribution functions of the adsorption energy sites of *n*-hexylamine and *n*-octane on K673 fiber. One can see that the distribution function of *n*-hexylamine is very distinct from that of *n*-octane. There are two peaks relatively narrow with peak position around 25 and 30 kJ/mol observed on the *n*-hexylamine probe, and the number of sites at higher adsorption energy increases considerably when comparing with the *n*-octane probe. This indicates that a strong specific interaction takes place between *n*-hexylamine and the surface of K673 fiber, most probably due to a hydrogen-bonding interaction with the oxygen-containing groups on the less crystalline region. However, there is no specific interaction occurring between *n*-octane and the Kevlar® fiber surface, because the inert *n*-octane molecules have no access for a specific interaction, such as hydrogen-bonding or dipole–dipole interaction, with the Kevlar®

fiber surface. The features of two peaks appearing in an energy density distribution function from *n*-hexylamine adsorption suggest the existence of two types of interaction with Kevlar® fiber, i.e. the universal van der Waals force and specific hydrogen-bonding interaction, and therewith the availability of two morphologically different regions to interact with. The increase in the number of sites when using *n*-hexylamine as compared with *n*-octane could be contributed from two parts, one is due to the molecular affinity on the fiber surface, and the other reason is that the molecular size of *n*-hexylamine is smaller than *n*-octane.

In the case of *n*-octane probe adsorption seen in Fig. 6(b), there is a point (energy site) positioned at 21.5 kJ/mol with an extremely high distribution percentage, 35.0 mol^2/Jm$^2 \times 10^{10}$, when compared with other energy sites possessing very low distribution values in the range of 0–1 mol^2/Jm$^2 \times 10^{10}$. This high distribution energy value agrees very well with the surface free energy of adsorption measured at infinite dilution (21.3 kJ/mol). It indicates that the Kevlar® surface is quite homogeneous in energy sites distribution in response to the alkane molecules, such as *n*-octane, mainly originated from a van der Waals force interaction.
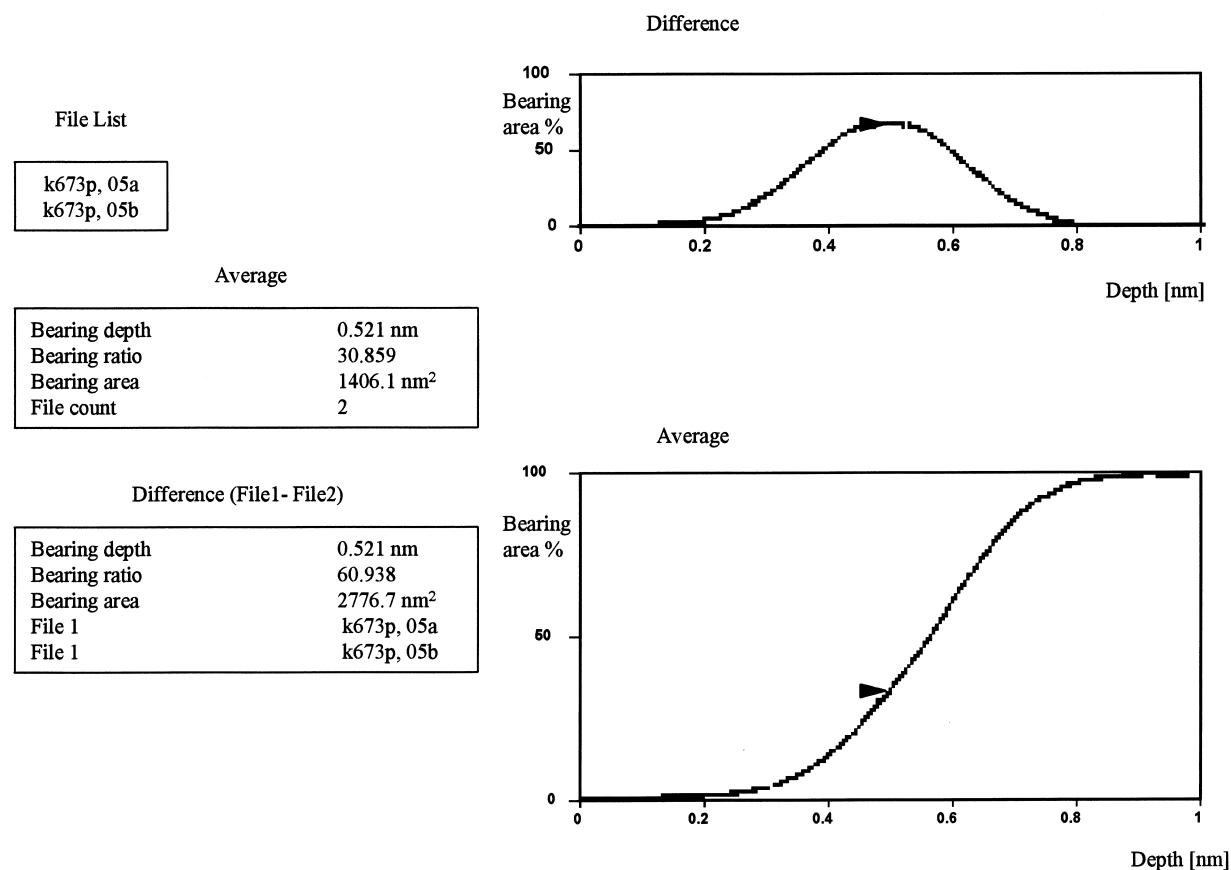
(c)

Bearing Compare

File List

| k673p, 05a |
| k673p, 05b |

Average

Bearing depth	0.521 nm
Bearing ratio	30.859
Bearing area	1406.1 nm²
File count	2

Difference (File1- File2)

Bearing depth	0.521 nm
Bearing ratio	60.938
Bearing area	2776.7 nm²
File 1	k673p, 05a
File 1	k673p, 05b

Difference

Average

Fig. 5. (*continued*)

4. Conclusion

The Kevlar® structure presented above by the AFM tapping mode analysis gives a reliable information on the fiber surface structure features, due to the minimized deformation between the tip and samples. The microfibrils feature due to the manufacture spinning process was observed with an average width of 500 nm. The microfibrils are composed of various types of pleated periodical structures of an average size 50 nm. The skin-core-like differentiation was observed in a less crystalline zone on the surface where the periodical units are arranged disorderly with a certain degree of layers overlap. However, in a highly crystalline zone, the repeated units are more uniformly arranged in a rectangular network manner.

The surface energy of Kevlar® fiber is strongly related to its surface structure. For example, a less crystalline spot such as the skin-core-like zone described above has defects and voids and could be the place of a higher surface energy region due to a possible hydrogen-bonding or other types of dipole interactions. In contrast, a highly crystalline zone normally posses a lower surface energy via van der Waals force because of an ordered and less defect structure. The IGC results at finite concentration, the polar probe n-hexylamine exhibits a distinct two-peaks adsorption curves on the K673 fiber surfaces. These IGC data could be correlated to the AFM observation. The energy distribution function is more heterogeneously and high energetically spread for n-hexylamine due to a possible hydrogen-bonding or polar interaction with the oxygen-containing groups adsorbed on the less crystalline spot. However, the adsorption curve is low and homogeneous for n-octane, because this inert molecule has no excess to further interact with the defect structure on the Kevlar® fiber surface.

The scheme shown in Fig. 7 in regard to the periodical structure pleated arrangement of Kevlar® fibers is proposed based on our AFM observations and IGC surface energy investigation. We suggested that the impurities or moisture could be more easily adsorbed on the less crystalline region of heterogeneous structure than onto the homogeneous organization at the highly crystalline zone [19]. The different patterns of periodical organizations on the fiber surface may be caused from several parameters such as the fiber formation and spinning condition (spinning force, spinning

(a)

Hexylamine at 50°C on Fibre K673

(b)
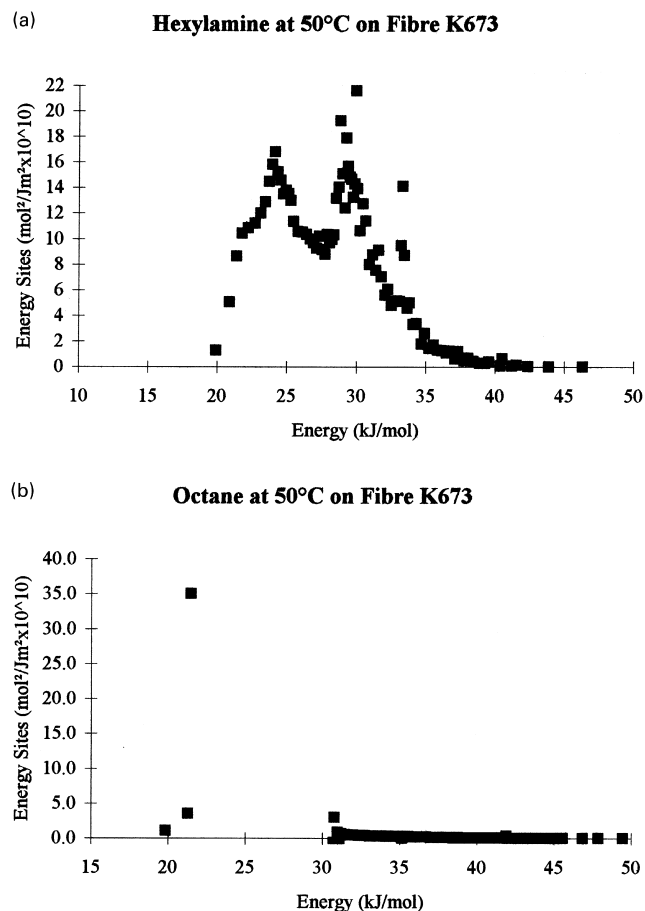
Octane at 50°C on Fibre K673

Fig. 6. Energy distribution function obtained by finite concentration method of (a) *n*-hexylamine; (b) *n*-octane adsorbed on Kevlar® K673 fiber at 50°C.

Kevlar® fiber filament

Fig. 7. A proposed microfibril and pleated appearance of periodical structure arrangements on Kevlar® fiber surface.

rate and the spin-head configuration) of manufacturing process. The less crystalline region has more voids and defects on it and oxygen-containing groups could be formed there, thus polar probes such as hexylamine could be strongly interacted with.

References

[1] Penn L, Larson F. J Appl Polym Sci 1979;23:59.
[2] Yang HH. Aromatic high-strength fibers Ch. II. New York: Wiley, 1989.
[3] Blades H. US Patent 3,767756, 1973.
[4] Dobb MG, Johnson DJ, Saville BP. J Polym Sci, Polym Phys Ed 1977;15:2201.
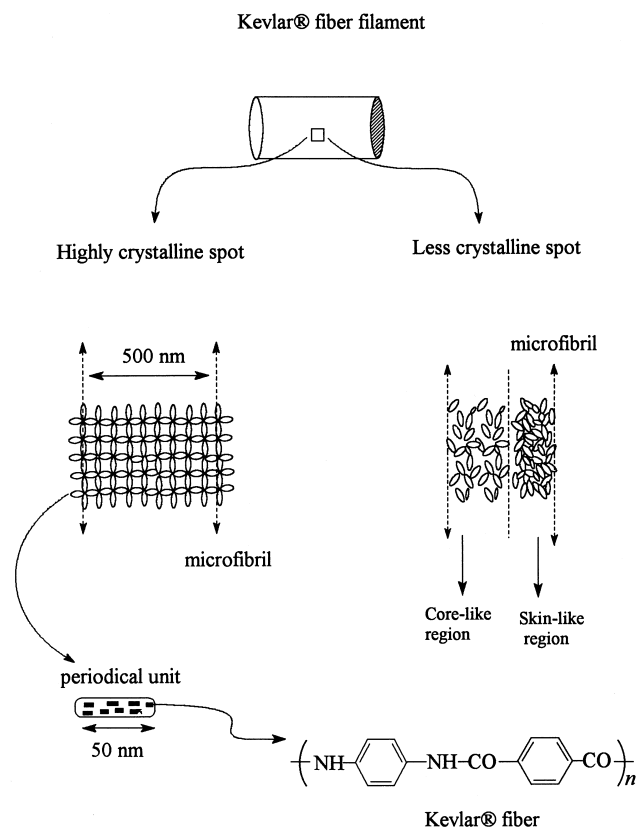[5] Hagege R, Jarrin M, Sutton M. J Microscopy 1979;115:65.
[6] Li LS, Allard LF, Bigelow WC. J Macromol Sci Phys 1983;B22(2):269.
[7] Penn L, Larson F. J Appl Polym Sci 1979;23:59.
[8] Snétivy D, Vancso GJ, Rutledge GC. Macromolecules 1992;25:7037.
[9] Li SFY, McGhi AJ, Tang SL. Polymer 1993;34:4573.
[10] Rebouillat S, Donnet JB, Wang TK. Polymer 1997;38:2245.
[11] Snétivy D, Yang H, Vancso GJ. J Mater Chem 1992;2:891.
[12] Magonov SN, Reneker DH. Ann Rev Mater Sci 1997;27:175.
[13] Panar M, Avakian P, Blume RC, Gardner KH, Gierke TD, Yang HH. J Polym Sci, Polym Phys Ed 1983;21:1995.
[14] Rebouillat S, Escoubes M, Gauthier R, Vigier A. J Appl Polym Sci 1995;58:1305.
[15] Rebouillat S, Donnet JB, Guo H, Wang TK. J Appl Polym Sci 1998;67:487.
[16] Robson JP. Can J Phy 1965;43:1941.
[17] Rudzinski W, Everett DH. Adsorption of gases on heterogeneous surface. London: Academic Press, 1992.
[18] Conder JR, Young CL. Physicochemical measurements by chromatography. New York: Wiley, 1979.
[19] Morgan RJ, Pruneda CA, Steele WJ. J Polym Sci, Polym Phys Ed 1983;21:1757.